

MISSION ANALYSIS OF DETECTING DEBRIS WITH A NEAR-INFRARED SYNTHETIC APERTURE RADAR SATELLITE

Matsuura Seiga⁽¹⁾, Kogi Yuichiro⁽²⁾, Mase Atsushi⁽³⁾, Hatta Shinji⁽⁴⁾, and Hanada Toshiya⁽⁵⁾

⁽¹⁾Kyushu University, Fukuoka, Japan, Email: matsuura.seiga.656@s.kyushu-u.ac.jp

⁽²⁾Fukuoka Institute of Technology, Fukuoka, Japan, Email: kogi@fit.ac.jp

⁽³⁾Masehira Co., Ltd., Fukuoka, Japan, Email: mase.atsushi.510@m.kyushu-u.ac.jp

⁽⁴⁾MUSCAT Space Engineering Co., Ltd., Fukuoka, Japan, Email: hatta@astro-muse.com

⁽⁵⁾Kyushu University, Fukuoka, Japan, Email: hanada.toshiya.293@m.kyushu-u.ac.jp

ABSTRACT

This study proposes a near-infrared synthetic aperture radar (SAR) satellite to detect debris between 5 cm and 1 m in size in geostationary orbit (GEO). The near-infrared SAR proposed here is capable of detecting 5 cm and larger objects passing within a range of 50 km that have not been cataloged and therefore have posed a threat to operational geosynchronous spacecraft. However, the initial aim is kept to verify the detection capabilities of near-infrared SAR in low-Earth orbit (LEO) rather than GEO, since launch opportunities into GEO are quite limited and expensive, and 10 cm and large objects in LEO are cataloged, making the verification ideal and promising. The detection principle of the near-infrared SAR and the outcome of the mission analysis for technology demonstration are described below.

Traditional ground-based optical observations can detect debris of 10 cm or larger. The infrared SAR proposed here is capable of observing debris from 5 cm to 10 cm. In the 1st stage, debris orbital data is measured by a laser radar system with two-laser scan-planes set by some azimuth angle shift. This system measures two positions at each detected time and estimates orbital data. Then, in the 2nd stage, a laser SAR system visualizes debris with a resolution of 5 cm. The laser SAR system projects and locks a beam to the debris during the measurement using a laser scanning system and pre-measured orbital data. The laser SAR collects reflected laser beams from a wide look angle adequate for computing a debris image with a resolution of 5 cm. This advancement enables cataloging smaller debris than previously, contributing significantly to cataloging uncataloged objects.

Then, this study examines the approach between the observation satellite and debris and assesses the likelihood of observability based on incoming direction and relative speed. To evaluate observability, it is required that the debris cross the laser observation field at a relative speed of 1km/s or lower to detect with the laser SAR. As another condition, it is assumed that the observation satellite is in a sun-synchronous orbit at an altitude of 800 km, with debris data designated as “OBJECTtype: Debris”

and “RCS: Small” in the catalog. This study evaluates the number of debris passing through the radar field at relative speeds detectable over a one-year mission duration.

As a result, it is found that many debris approach from the desired direction, and that the relative speed is slow enough. Therefore, it is concluded that plenty of observation opportunities exist for system validation during the mission.

Keywords: near-infrared synthetic aperture radar; space surveillance; geostationary region; technology demonstration.

1. INTRODUCTION

Since the launch of Sputnik 1 in 1957, space exploration has advanced significantly. However, many inactive satellites and rocket debris remain in orbit as space debris. Additionally, debris is generated through collisions between existing debris, leading to a continuous increase in the number of debris objects.

Figure.1 illustrates the future trend of debris population under two scenarios: one without active debris removal and another where 90 percent of decommissioned satellites are deorbited. The results indicate that to stabilize the debris population, at least five decommissioned satellites must be removed from orbit annually. Collisions with such debris can result in catastrophic consequences [5].

Traditionally, debris observation has primarily been conducted from the ground. However, using this method, only debris larger than 1 meter can be observed in geostationary orbit, making detection difficult. Therefore, it is necessary to catalog debris smaller than 1 meter in geostationary orbit.

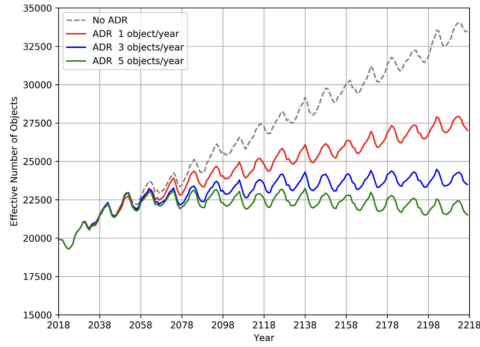


Figure 1. Future debris population scenarios under different active debris removal (ADR) conditions [2]

2. OBSERVATION METHOD

2.1. Microwave-modulated infrared laser radar/SAR

A microwave-modulated infrared laser radar as shown in Fig. 2 is designed and fabricated for improvement of the spatial resolution both in the range direction and the azimuth direction. There are several benefits in the radar diagnostics using this system. For example, speckle is one of the serious problems for obtaining good signal to noise ratio in the microwave region. This problem can be eliminated because an IR laser output is used as a carrier wave. The drop of coherence length which becomes a problem in laser radar can also be neglected since the data processing is performed in modulated microwave region. An infrared wave (1550 nm, 1–30 W) is modulated by an output of a chirp oscillator with frequency of 1-18 GHz. The modulated wave is amplified by a fiber amplifier and irradiated by a transmitting optics. The reflected wave from an object is picked up by a receiving optics and fed to an optics detector and a demodulator. Transmitting/receiving lights are scanned by using a rotation mirror and a gimbal rotor stage. In proof-of-principle experiment, a spatial resolution of 1 cm has been achieved in laser radar or laser SAR operation [4,6].

2.2. Two operation modes for debris detection

The laser radar system has scan mode (A) and SAR mode (B) as shown in Fig. 3. The scan mode is used to detect small unsampled debris (5-10 cm). It detects the location and transit times of debris in the two observation planes, leading to the calculation of its orbital data. The SAR mode is used to visualize pre-sampled objects. The laser radar system collects reflection data while locking the beam on the objects, and reconstructs the images by means of inverse SAR technology.

We are now designing optical head for the scan mode. The scanning mode of the laser radar uses an optical

system that scans the projection beam and the receiving beam in the range-elevation cross-sectional plane. The projection beam irradiates debris, and its reflected beam is received by the receiving optics. Here, the divergence of the beams, the angular velocity of the elevation scan, the scattering cross section of the detectable debris, velocity of the detectable debris, and detectable range of the debris are affected to each other, and in trade-off relationships. Fig. 4 shows a simulation example of the area in which propagation beam (within the red lines) and detectable reflected beam (within the blue lines) in a range-elevation cross section. Here, the divergence angle of the transmitted and received beams are set to 0.05 rad and 0.15 rad, respectively. The elevation scan angular velocity is set to 0.3 mrad/ μ s. In order to detect the reflected light from debris, the projection beam area must be inside the detectable receiver area, as shown in the figure. Since the beam is scanned in the elevation direction in time, the projection area and receiving area are not simply fan shape but a curved shape as shown in the figure. To detect faster debris, it is necessary to increase the elevation scan angular velocity. However, the degree of curvature of the beams increases accordingly, thus there is some limit to narrowing the receiver area. Furthermore, in order to detect debris with a small scattering cross section, the beam divergence must be narrowed to increase the gain, however, there is some limit to narrowing the reception area for the same reason. In the present design, the laser radar system can detect debris with velocity less than 1km/s at a range of 50 km. We will investigate the relationship between the output of the entire system and the scattering cross-sectional of debris, and optimize the system specifications in the near future.

3. EVALUATION OF OBSERVABILITY

In this section, we describe the analytical methods used to examine the number of approaching debris [1].

3.1. Coordinate Systems

In this study, we primarily discuss the following two coordinate systems.

IJK Coordinate System

As shown in Fig. 5, this is an Earth-fixed coordinate system where the I-axis points toward the vernal equinox, the K-axis points toward the North Pole, and the J-axis is defined to form a right-handed coordinate system with the other two axes.

NTW Coordinate System

As shown in Fig. 6, this is a coordinate system fixed to a spacecraft in orbit. The T-axis aligns with the velocity vector of the spacecraft, the W-axis aligns with the orbital angular momentum vector, and the N-axis is defined to form a right-handed coordinate system with

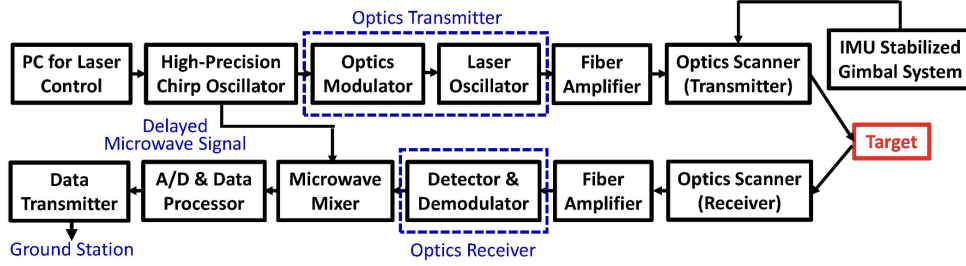


Figure 2. Schematic of a microwave-modulated infrared laser radar/SAR.

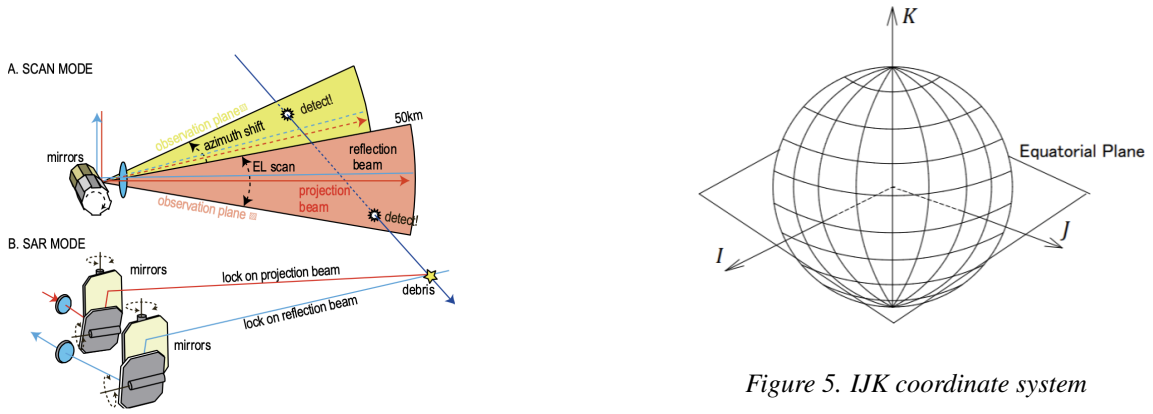


Figure 3. Beam steering and optical heads of the laser radar system in the scan mode (A) and the SAR mode (B)

the other two axes [3].

By performing proximity analysis, we can determine the position and relative velocity of both the observation satellite and debris in the IJK space at the time of closest approach. These values can be expressed as vectors as follows:

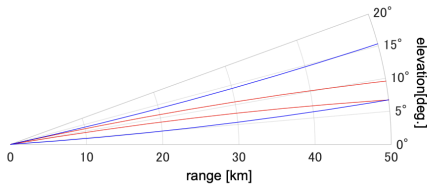


Figure 4. The divergence of the projection beam(red) and receiver beam(blue) in the range-elevation cross-sectional plane.

$$\mathbf{r}_{S/C} = \begin{pmatrix} x_1 \\ y_1 \\ z_1 \end{pmatrix} \quad (1)$$

$$\mathbf{r}_{DEB} = \begin{pmatrix} x_2 \\ y_2 \\ z_2 \end{pmatrix} \quad (2)$$

$$\mathbf{v}_{S/C} = \begin{pmatrix} v_{x1} \\ v_{y1} \\ v_{z1} \end{pmatrix} \quad (3)$$

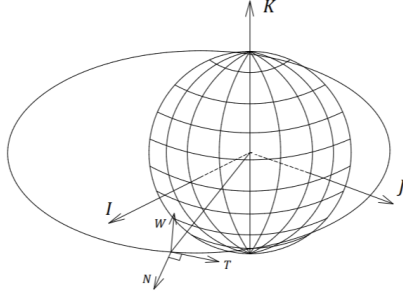


Figure 6. NTW coordinate system

$$\mathbf{v}_{DEB} = \begin{pmatrix} v_{x2} \\ v_{y2} \\ v_{z2} \end{pmatrix} \quad (4)$$

Here, the relative position and relative velocity of the debris with respect to the observation satellite in the IJK coordinate system can be expressed as:

$$\mathbf{r}_{IJKrel} = \mathbf{r}_{DEB} - \mathbf{r}_{S/C} \quad (5)$$

$$\mathbf{v}_{IJKrel} = \mathbf{v}_{DEB} - \mathbf{v}_{S/C} \quad (6)$$

On the other hand, the axes of the NTW coordinate system are defined as follows: First, the T-axis coincides with the velocity vector of the observation satellite:

$$\mathbf{T} = \frac{\mathbf{v}_{S/C}}{|\mathbf{v}_{S/C}|} \quad (7)$$

Similarly, the W-axis is aligned with the orbital angular momentum vector:

$$\mathbf{W} = \frac{\mathbf{r}_{S/C}}{|\mathbf{r}_{S/C}|} \times \frac{\mathbf{v}_{S/C}}{|\mathbf{v}_{S/C}|} \quad (8)$$

The N-axis is defined to form a right-handed coordinate system with the T and W axes:

$$\mathbf{N} = \mathbf{T} \times \mathbf{W} \quad (9)$$

Using these unit vectors, the relative position and relative velocity vectors in the IJK coordinate system can be transformed as follows:

$$\mathbf{r}_{rel} = \begin{pmatrix} \mathbf{r}_{IJKrel} \cdot \mathbf{N} \\ \mathbf{r}_{IJKrel} \cdot \mathbf{T} \\ \mathbf{r}_{IJKrel} \cdot \mathbf{W} \end{pmatrix} \quad (10)$$

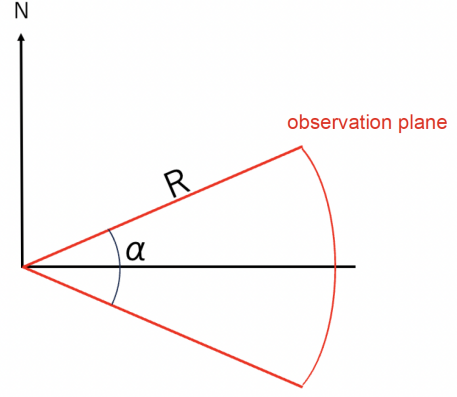


Figure 7. Definition of observation plane

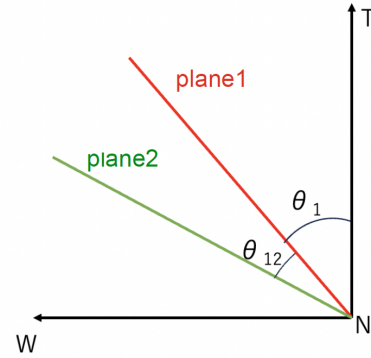


Figure 8. Configuration of observation planes

$$\mathbf{v}_{rel} = \begin{pmatrix} \mathbf{v}_{IJKrel} \cdot \mathbf{N} \\ \mathbf{v}_{IJKrel} \cdot \mathbf{T} \\ \mathbf{v}_{IJKrel} \cdot \mathbf{W} \end{pmatrix} \quad (11)$$

The values of r_{rel} and v_{rel} obtained here can be used to calculate debris that meets specific conditions.

3.2. Observation Range

As shown in Fig. 7, the maximum detectable radius of the observation plane is denoted as R , and the scan angle as α . The scan plane is perpendicular to the TW plane, and as illustrated in Fig. 8, the angle between the T-axis and the first observation plane in the TW plane is denoted as θ_1 , while the angle between the first and second observation planes is θ_{12} .

3.3. Detection Criteria

To determine whether debris is detectable, the following conditions are used. As explained, the relative position

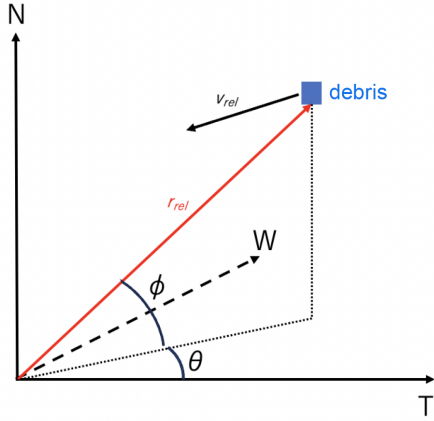


Figure 9. Definition of debris coordinate

and velocity of debris in the NTW coordinate system can be obtained from the results of proximity analysis. Using these values, the debris trajectory in the NTW coordinate system is expressed as follows:

$$\mathbf{L} = \mathbf{r}_{rel} + \mathbf{v}_{rel} \cdot t \quad (12)$$

where

$$\mathbf{r}_{rel} = \begin{pmatrix} x_0 \\ y_0 \\ z_0 \end{pmatrix} \quad (13)$$

$$\mathbf{v}_{rel} = \begin{pmatrix} v_x \\ v_y \\ v_z \end{pmatrix} \quad (14)$$

Furthermore, as shown in Fig. 9, the coordinates of debris can be expressed in spherical coordinates as follows:

$$\begin{aligned} x &= r \cos \theta \cos \phi \\ y &= r \sin \theta \cos \phi \\ z &= r \sin \phi \end{aligned} \quad (15)$$

From Eqs. 12 and 15, the following equalities hold:

$$\begin{aligned} r \cos \theta \cos \phi &= x_0 + v_x t \\ r \sin \theta \cos \phi &= y_0 + v_y t \\ r \sin \phi &= z_0 + v_z t \end{aligned} \quad (16)$$

At any given time t , the relative position of the debris is given by:

$$r = \sqrt{(x_0 + v_x t)^2 + (y_0 + v_y t)^2 + (z_0 + v_z t)^2} \quad (17)$$

Here, if the azimuth angle of the near-infrared SAR is θ_1 and the relative position of the debris lies on the radar plane, the following two conditions must be satisfied:

$$|\phi| < \frac{\alpha}{2} \quad (18)$$

$$r < R \quad (19)$$

When the relative position of the debris coincides with the observation plane, meaning that the azimuth angle of the debris is θ_1 , we obtain:

$$\tan \theta_1 = \frac{y_0 + v_y t}{x_0 + v_x t} \quad (20)$$

Solving for t :

$$t = \frac{x_0 \tan \theta_1 - y_0}{v_y - v_x \tan \theta_1} \quad (21)$$

provided that:

$$v_y - v_x \tan \theta_1 \neq 0 \quad (22)$$

At this moment, the relative elevation angle ϕ of the debris is given by:

$$\phi = \arctan \frac{z}{x^2 + y^2} \quad (23)$$

Substituting the trajectory equation:

$$\phi = \arctan \frac{z_0 + v_z t}{\sqrt{(x_0 + v_x t)^2 + (y_0 + v_y t)^2}} \quad (24)$$

By substituting t from Eq. 21, we obtain the value of ϕ .

Additionally, the velocity of the debris when passing through the observation plane must also be considered as a detection condition. The velocity component of the debris perpendicular to the radar plane, denoted as v_{ver} , is determined as follows.

The normal vector of the observation plane is given by:

$$\mathbf{n} = \begin{pmatrix} \sin \theta_1 \\ -\cos \theta_1 \\ 0 \end{pmatrix} \quad (25)$$

Using this normal vector, the velocity component perpendicular to the observation plane is given by:

Table 1. Definition of debris size based on radar cross section (RCS)

Bin	RCS[m ²]
Small	RCS < 0.1
Middle	0.1 ≤ RCS < 1.0
Large	1.0 ≤ RCS

Table 2. Observation Satellite Orbit

Perigee Altitude [km]	800
Apogee Altitude [km]	800
Orbital Inclination [deg]	98.576

$$\mathbf{v}_{ver} = \left(\frac{\mathbf{v}_{rel} \cdot \mathbf{n}}{\|\mathbf{n}\|^2} \right) \cdot \mathbf{n} \quad (26)$$

Expanding this expression:

$$\mathbf{v}_{ver} = \begin{pmatrix} (v_x \sin \theta_1 - v_y \cos \theta_1) \sin \theta_1 \\ -(v_x \sin \theta_1 - v_y \cos \theta_1) \cos \theta_1 \\ 0 \end{pmatrix} \quad (27)$$

This equation determines the perpendicular velocity component, which serves as a criterion for debris detection.

3.4. Analysis Conditions

For the analysis, the target debris is defined as "Small" based on the radar cross section (RCS), as shown in Tab. 1. While "Middle" debris is also of interest, this study focuses on evaluating the observation frequency of "Small" debris, which is more challenging to detect.

Additionally, the observation satellite is assumed to be in a Sun-synchronous orbit at an altitude of approximately 800 km, as described in Tab. 2.

Furthermore, the conditions of the near-infrared SAR are set as shown in Tab. 3.

In the following discussion, we will examine how the azimuth angle θ_1 of the near-infrared SAR, the angle θ_{12} between the two observation planes, and the field of view angle α affect the number of observable debris.

Table 3. Near-Infrared SAR Conditions

Maximum Detection Range R [km]	50
Near-Infrared SAR Elevation Angle	0
ϕ_1 [deg]	

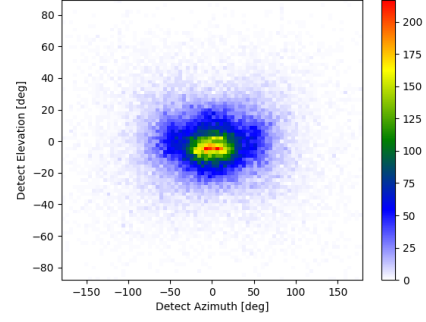


Figure 10. Two-dimensional histogram of detected debris positions

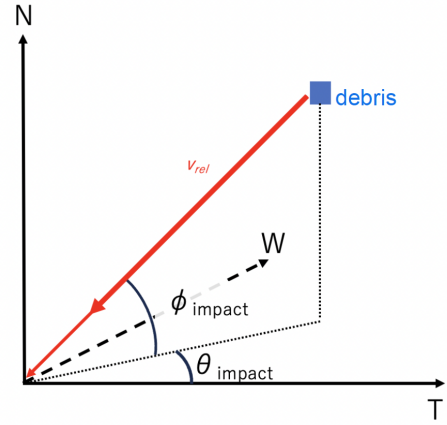


Figure 11. Definition of incoming direction

3.5. Analysis Results

As a result of the proximity analysis, the detection positions of debris in the NTW coordinate system were obtained, as shown in Fig. 10. The histogram indicates that detections are concentrated near an azimuth and elevation of 0 degrees.

Next, the flight direction of debris is defined as shown in Fig. 11. The azimuth angle of the incoming direction θ_{im} is plotted on the horizontal axis, and the elevation angle ϕ_{im} is plotted on the vertical axis. The number of debris arriving from each direction is represented as a two-dimensional histogram in Fig. 12.

The results show that most debris has a directional vector indicating that it is arriving from the front. Debris coming from the front generally has a relatively high relative velocity.

Next, we calculate the number of debris that can be observed at different elevation angles θ_1 of the near-infrared SAR and discuss the optimal installation orientation. We also examine how the number of observable debris changes depending on the angle θ_{12} between the two observation planes and the field of view angle α of

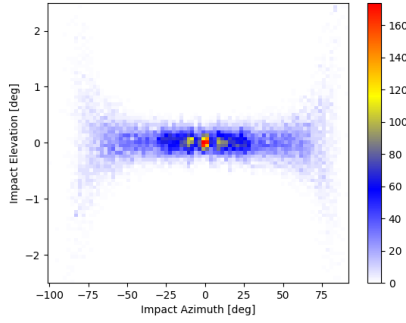


Figure 12. Two-dimensional histogram of incoming direction of detected debris

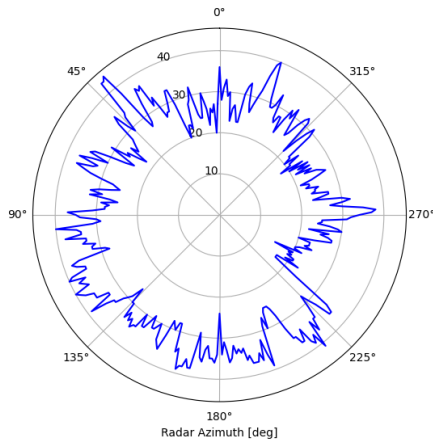


Figure 13. Case of $\theta_{12} = 0.1$ [deg], $\alpha = 15$ [deg]

the observation plane.

First, we consider the case where $\theta_{12} = 0.1$ [deg] and $\alpha = 15$ [deg]. The relationship between θ_1 and the number of observable debris is shown in Fig. 13.

From this figure, it is evident that there are localized increases in the number of observable debris, but an overall trend is not visible. This indicates that debris can be observed regardless of the orientation of the near-infrared SAR.

Next, when $\theta_1 = 0$ [deg], the locations where debris was detected within the observation plane are shown in Fig. 14.

The black frame represents the observation area, blue dots indicate debris that passed through regardless of velocity, and red dots indicate debris that passed through while satisfying the velocity condition. From this figure, it can be seen that there is no bias in the locations where debris passes through the observation area. This suggests that as the detectable distance increases, the number of observable debris increases in proportion to the square of that distance.

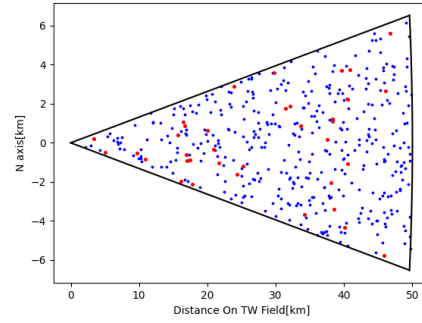


Figure 14. Detected debris positions within the observation plane

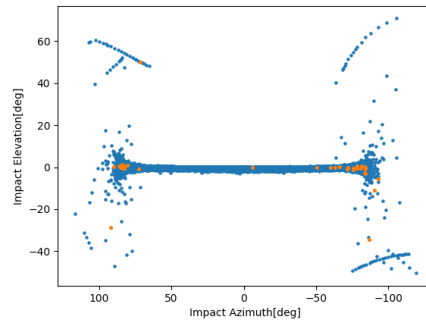


Figure 15. Incoming direction of detected debris

Additionally, Figs. 15 and 16 show the debris detected in the proximity analysis (blue dots), and the debris that satisfies the analysis conditions and can be observed by radar (orange dots). These figures indicate that most of the detectable debris arrives in a direction perpendicular to the flight direction. The reason for this is that debris arriving from a perpendicular direction has an orbit close to that of the observation satellite, resulting in a lower relative velocity at close approach.

Next, we increase the value of θ_{12} and examine the case of $\theta_{12} = 1$ [deg] and $\alpha = 15$ [deg]. The relationship between θ_1 and the number of observable debris in this case is shown in Fig. 17.

Similarly, we consider the case where $\theta_{12} = 5$ [deg] and $\alpha = 15$ [deg], further increasing the angle between the two observation planes. The relationship between θ_1 and the number of observable debris in this case is shown in Fig. 18.

From these graphs, it is clear that increasing the spacing between the two planes reduces the number of observable debris. On the other hand, the number of observable debris at each orientation follows a similar trend regardless of the value of θ_{12} .

Next, we consider the case where $\theta_{12} = 0.1$ [deg] is fixed and the field of view angle of the observation plane is

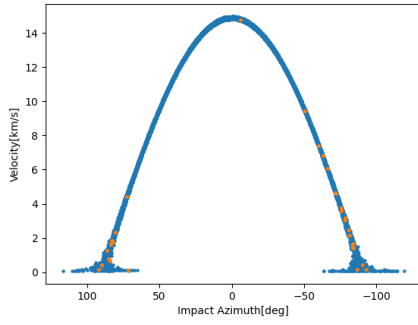


Figure 16. Elevation angle and relative velocity of detected debris

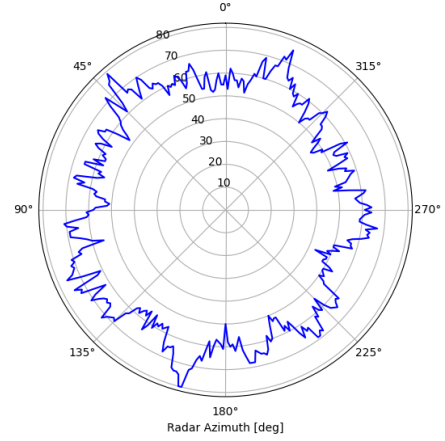


Figure 19. Case of $\theta_{12} = 0.1$ [deg], $\alpha = 30$ [deg]

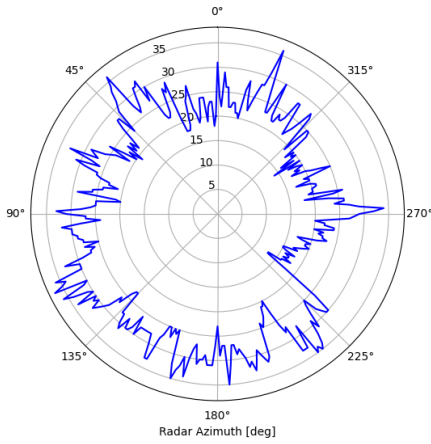


Figure 17. Case of $\theta_{12} = 1$ [deg], $\alpha = 15$ [deg]

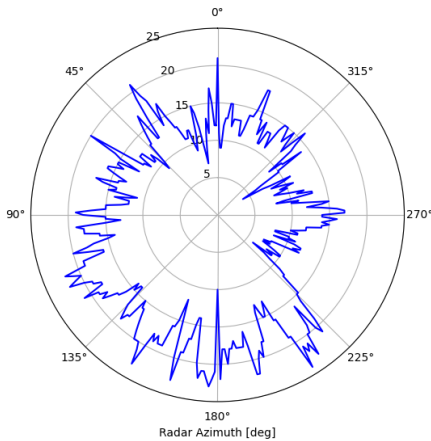


Figure 18. Case of $\theta_{12} = 5$ [deg], $\alpha = 15$ [deg]

increased.

As discussed earlier, since debris passes through the observation plane without bias, the number of observable debris increases proportionally with the field of view angle.

CONCLUSION

In this paper, we first conducted a proximity analysis to examine how closely debris approaches the observation satellite and to determine its velocity and positional relationship. The results showed that the closest approach of debris occurs in the direction of the observation satellite's motion. Additionally, the analysis indicated that most debris arrives from the front.

Furthermore, based on the position and velocity of the debris, we investigated how the number of debris passing through the observation plane changes by considering parameters such as the field of view, the angle between observation planes, and the orientation of the radar. The results demonstrated that increasing the field of view proportionally increases the number of observable debris. However, design constraints also become more significant, necessitating a discussion that accounts for these limitations.

Additionally, a smaller angle between observation planes increases the number of observable debris. However, in such cases, it is necessary to estimate the velocity of unknown debris based on the positions of the passage points. Therefore, an optimal design must be determined while considering these factors.

REFERENCES

1. Curtis H. D., (2020). *Orbital Mechanics for Engineering Students*, ELSEVIER, Revised Fourth Edition.
2. Kawamoto S., Nagaoka N., Sato T., Hanada T., (2020). Impact on collision probability by post mission disposal and active debris removal, *Journal of Space Safety Engineering*, **7**(3), 178–191.
3. Isobe H., (2021). Formation keeping with simultaneous orbital departure from non-cooperative objects, *Bachelor Thesis, Kyushu University*.
4. Mase A. et al., (2018). *Adv. Phys. X*, **3**, 633–675, DOI: 10.1080/23746149.2018.1472529.
5. Tagawa M., (2014). System Combining Space- and Ground-based Sensors to Track Small Objects in Low Earth Orbit, *Ph.D Thesis, Kyushu University*.
6. Kogi Y. et al., (2022). *Appl. Sci.*, **12**, 9836–9845, DOI: 10.3390/app12199836.